PRACTICAL STAND OFF DAMPING TREATMENT FOR SHEET METAL

Mr. Michael L. Parin
Visiting Scientist
WRDC/FIBA
Wright-Patterson AFB, OH 45433
(513) 255-5664
Formally of Anatrol Corporation
Cincinnati, Oh 45241

Dr. Lynn Rogers
WRDC/FIBA
Wright-Patterson AFB, OH 45433
(513) 255-5664

Dr. Young In Moon
Anamet Laboratories, Inc.
P. O. Box 31041
Overlook Branch
Dayton, OH 45431
(513) 252-1630

Mr. Michael Falugi
Anamet Laboratories, Inc.
P. O. Box 31041
Overlook Branch
Dayton, OH 45431
(513) 252-1630

FOR DAMPING '89, FEB 8-10, 1989
THE PALM HOTEL, WEST PALM BEACH, FLORIDA

ABSTRACT

The impressive potential of Stand-Off-Damping (SOD) systems (historically referred to as "spaced" damping treatments) to control structural resonant response levels has long been recognized. However, the inability to identify materials that store virtually no bending energy while transferring significant shear loads has essentially rendered this concept an academic novelty.

This paper presents analytical and experimental results of a study conducted to investigate a practical SOD system. The analysis for a simply supported four layer beam system, consisting of: 1) a base structure; 2) a stand-off layer; 3) a dissipative viscoelastic layer; and 4) a constraining layer are presented. The numerical results of a limited parametric study to investigate the relationship between the Stand-Off layer, damping layer, and constraining layer geometries and modulus values are presented. Computer generated plots of modal loss factor, RMS response ratio, peak response ratios, and frequency ratios as a function of temperature for a damped and undamped test case are reviewed. Finally, experimental test results of modal loss factor for a conventional three layer damping system and a SOD system are compared to the predicted values for a generic test article.

1.0 INTRODUCTION

Of the many critical design criteria by which modern military and civilian aircraft are designed and manufactured, those related to the dynamic behaviors of the structure are the most difficult to quantify prior to actual use of the aircraft. Specifically, fatigue failure from high-frequency vibration and acoustic noise can occur at many locations in the secondary structure; yet the determination of location and magnitude of structural response is usually obtained from component or full-scale tests. The usual consequence of finding undesirable dynamic behavior is either to redesign the structure, which is expensive, or modify it with additional structural stiffeners.

Another acceptable remedy to reduce the damaging effects of high-frequency vibration is to provide a local damping treatment of suitable density and distribution to reduce the overall amplitude. Because damping materials add weight they must, of necessity, be properly designed to achieve the required level of damping at a minimum increase in vehicle weight.

The use of viscoelastic damping materials (VEM) in constrained layers is an established technique for reducing resonant structural vibration [1,2,7,8]. However, the proper design of viscoelastic damped structures requires proven methods and techniques that have application to both new and existing aircraft structures. Some of these methods have been developed by the Wright Research and Development Center (WRDC), the Aerospace Structures Information and Analysis Center (ASIAC), and Anatrol Corporation.

The objective of any constrained-layer damping treatment is to dissipate vibration energy by deforming viscoelastic materials. In the deformation process, the temperatures of the damping materials increase because they remove kinetic energy from the total system. For structural systems which experience relatively large bending strains

without large deflections, the use of constrained layers which dissipate energy through the shearing of the viscoelastic layer is an accepted design approach.

Although there are two types of distributed damping systems, namely free layer and constrained layer, this paper is limited to an analysis of a variation on the conventional three (3) layer system illustrated in Figure 1a. The particular system considered is shown in Figure 1b and consists of a base structure, a Stand-Off layer, a dissipative viscoelastic layer, and a stiff constraining layer.

The advantage of a four layer system that employs a Stand-Off layer is illustrated in Figure 2. The Stand-Off layer provides a greater separation between the neutral axis of the base structure and that of the overall system. This Stand-Off configuration increases the shear deformation introduced into the viscoelastic layer via a kinematic amplifier technique which significantly increases the damping efficiency of the treatment. By selecting a lightweight/shear stiff material for the Stand-Off layer and then configuring it to minimize its bending stiffness and overall weight, an effective and practical Stand-Off layer was conceived.

2.0 DERIVATION OF GOVERNING EQUATIONS FOR FOUR-LAYER CONSTRAINED LAYER DAMPING SYSTEM

The four-layer simply supported beam model is depicted in Figure 3 with appropriate notations to be used in the derivation of the governing equations. The principal assumptions to be used are as follows:

1. Only bending and shear deformations are considered– in-plane extensional strains are assumed small and negligible.
2. Bending deformations, strains, and stresses are governed by classical Euler-Bernoulli beam theory [3].
3. Shear deformations (ϕ) of the base structure and constraining layer (k=1,4 in Figure 3) are the same. The principal shearing-energy dissipation mechanism occurs in the viscoelastic damping layer (k=3), since the shear stiffness of this layer is much less when compared to the other components' shear moduli.

Note, it is implicitly assumed that the structural and constraining layers are made of metallic materials, whereas the spacing and damping layers are made of polymeric compounds.

Additional assumptions required to complete the development will be presented as required.

The simple, one-dimensional analysis described below requires the determination of typical section properties; namely, centroid location, Z , and equivalent section stiffness, $\overline{EI}$. From Figure 3,

$$Z_c = \frac{H_1}{2} + Z_d \tag{1}$$

where Z_d is the distance from the mid-plane of the structural layer to the section centroid. The strains in each layer are found from:

$$\epsilon_1 = Z_d \phi' \tag{2}$$

$$\epsilon_2 = Z_2\phi' - \frac{t_2}{2}\psi_1' \tag{3}$$

$$\epsilon_3 = Z_3\phi' - (t_2 + \frac{t_3}{2})\psi_1' - \frac{t_3}{2}\psi_2' \tag{4}$$

$$\epsilon_4 = Z_4\phi' - (t_2 + t_3)\psi_1' - t_3\psi_2' \tag{5}$$

where the prime represents differentiation with respect to x. The corresponding forces in each layer are:

$$F_1 = E_1\epsilon_1 t_1 = X_1 Z_d\phi' \tag{6}$$

$$F_2 = E_2\epsilon_2 t_2 = X_2(Z_2\phi' - \frac{t_2}{2}\psi_1') \tag{7}$$

$$F_3 = X_3(Z_3\phi' - (t_2 + \frac{t_3}{2})\psi_1' - \frac{t_3}{2}\psi_2') \tag{8}$$

$$F_4 = X_4(Z_4\phi' - (t_2 + t_3)\psi_1' - t_3\psi_2') \tag{9}$$

where

$$X_k = E_k t_k \qquad k = 1,4 \tag{10}$$

and the strains ϵ_k are found from Equations (2)-(5). Applying the requirement for equilibrium of in-plane forces (and noting that the structural layer force, F_1, is compressive, whereas the other layers are in tension), i.e.,

$$\sum_{k=1}^{4} F_k = 0 \tag{11}$$

then

$$\begin{aligned} &-(X_1 + X_2 + X_3 + X_4)Z_d\phi' \\ &+(X_2(Z_2 + Z_d) + X_3(Z_3 + Z_d) + X_4(Z_4 + Z_d))\phi' \\ &-(t_2(\frac{X_2}{2} + X_3 + X_4) + t3(\frac{X_3}{2} + X_4))\psi_1' \\ &-t_3(\frac{X_3}{2} + X_4)\psi_2' = 0 \end{aligned} \tag{12}$$

From classical theory the centroidal location Z_c would normally be computed from Equation (12); however, the presence of ψ_1' and ψ_2' precludes this. In other words,

the section centroidal location depends on the shear that occurs in the spacing and damping layers.

To compute ψ_1' and ψ_2' the classical approach for computing shear stress is used [4], namely, based on equilibrium of the X-direction force and shear

$$F_4' = -G_3\psi_2 \tag{13}$$

and

$$F_3' + F_4' = -G_2\psi_1 \tag{14}$$

The quantities F_3' and F_4' are easily found from Equations (8) and (9).

At this point it is necessary to assume a sinusoidal mode shape in order to determine ψ_1 and ψ_2 consistent with the definition of loss factor presented in [5]. Assuming

$$w = sinKx \tag{15}$$

for simplicity, then

$$\phi = w' = KcosKx \tag{16}$$

$$\phi' = w'' = -K^2sinKx \tag{17}$$

and

$$\phi'' = w''' = -K^3cosKx \tag{18}$$

Assuming that ψ_1 and ψ_2 have the same distribution as w, then ψ_1 and ψ_2 are related to ϕ; that is

$$\psi_1 = \alpha_1\phi \tag{19}$$

and

$$\psi_2 = \alpha_2\phi \tag{20}$$

Through subsequent differentiations of Equations (19) and (20)

$$\alpha_1 = \frac{\psi_1'}{\phi'} = \frac{\psi_1''}{\phi''} \tag{21}$$

and

$$\alpha_2 = \frac{\psi_2'}{\phi'} = \frac{\psi_2''}{\phi''} \tag{22}$$

Returning to equations (13) and (14) and using the relations in Equations (16)-(22), Equation (13) can be written

$$S_{B1}\psi_1'' + S_{B2}\psi_2'' = S_{B3}\phi'' \tag{23}$$

$$S_{B1} = X_4(t_2 + t_3) \tag{24}$$

$$S_{B2} = (\frac{G_3}{K^2} + X_4 t_3) \tag{25}$$

and

$$S_{B3} = X_4 Z_4 \tag{26}$$

Similarly, Equation (14) is written

$$S_{A1}\psi_1'' + S_{A2}\psi_2'' = S_{A3}\phi'' \tag{27}$$

$$S_{A1} = X_3(t_2 + \frac{t_3}{2}) + X_4(t_2 + t_3) + \frac{G_2}{K^2} \tag{28}$$

where

$$S_{A2} = \frac{X_3 t_3}{2} + X_4 t_3 \tag{29}$$

and

$$S_{A3} = X_3 Z_3 + X_4 Z_4 \tag{30}$$

Equations (23) and (27) can be solved to provide

$$\psi_1'' = \left[\frac{S_{B3}S_{A2} - S_{B2}S_{A3}}{S_{B1}S_{A2} - S_{B2}S_{A1}}\right]\phi'' \tag{31}$$

and

$$\psi_2'' = \left[\frac{S_{B1}S_{A3} - S_{A1}S_{B3}}{S_{B1}S_{A2} - S_{A1}S_{B2}}\right]\phi'' \tag{32}$$

Observing Equations (21) and (22) and returning to Equation (12),

$$-P_A Z_d + P_B - P_C \alpha_1 - P_D \alpha_2 = 0 \tag{33}$$

where

$$P_A = X_1 + X_2 + X_3 + X_4 \tag{34}$$

$$P_B = X_2(Z_2 + Z_d) + X_3(Z_3 + Z_d) + X_4(Z_4 + Z_d) \tag{35}$$

$$P_C = t_2(\frac{X_2}{2} + X_3 + X_4) + t_3(\frac{X_3}{2} + X_4) \tag{36}$$

$$P_D = \frac{X_3}{2} + X_4 \tag{37}$$

Also, from Equations (31) and (32), with (21) and (22)

$$\alpha_1 = \frac{\psi_1'}{\phi'} = Y_A - Z_d Y_B \tag{38}$$

and

$$\alpha_2 = \frac{\psi_2'}{\phi'} = Y_C - Z_d Y_D \tag{39}$$

where

$$Y_A = \frac{S_{A2} X_4(Z_4 + Z_d) - S_{B2}(X_3(Z_3 + Z_D) + X_4(Z_4 + Z_d))}{\overline{S}} \tag{40}$$

$$Y_B = \frac{S_{A2} X_4 - S_{B2}(X_3 + X_4)}{\overline{S}} \tag{41}$$

$$Y_C = \frac{S_{B1}(X_3(Z_3 + Z_d) + X_4(Z_4 + Z_d)) - S_{A1}(X_4(Z_4 + Z_D)}{\overline{S}} \tag{42}$$

$$Y_D = \frac{S_{B1}(X_3 + X_4) - S_{A1} X_4}{\overline{S}} \tag{43}$$

and

$$\overline{S} = S_{B1} S_{A2} - S_{A1} S_{B2} \tag{44}$$

noting that

$$Z_2 + Z_d = \frac{1}{2}(t_1 + t_2) \tag{45}$$

and

$$Z_3 + Z_d = t_2 + \frac{1}{2}(t_1 + t_3) \tag{46}$$

$$Z_4 + Z_d = t_2 + t_3 + \frac{1}{2}(t_1 + t_4) \tag{47}$$

then Zd can be found from Equations (33)-(47) as

$$Z_d = \frac{P_C Y_A + P_D Y_C - P_B}{P_C Y_B + P_D Y_D - P_A} \tag{48}$$

If the section deformed with constant angle then the equation for the deflection curve can be represented in the following form:

$$\overline{EI}\phi' = M \tag{49}$$

where $\overline{EI}$ is the flexural rigidity and M is the bending moment of the beam. The total bending moment can be expressed as follows:

$$M = \sum_{k=1}^{4} M_{kk} + \sum_{k=1}^{4} F_k Z_k \tag{50}$$

where M_{kk} is the bending moment of the k^{th} layer

$$M_{kk} = \phi' E_k I_k \tag{51}$$

Equations (49) and (50) define the flexural rigidity as follows,

$$\begin{aligned}\overline{EI} &= E_1 I_1 + E_2 I_2 + E_3 I_3 + E_4 I_4 \\ &+ X_1 Z_d^2 + X_2 Z_2^2 + X_3 Z_3^2 + X_4 Z_4^2 \\ &- \left[E_2 I_2 + E_3 I_3 + \frac{X_2 t_2 Z_2}{2} + X_3(t_2 + \frac{t_3}{2}) Z_3 + X_4(t_2 + t_3) Z_4\right] \frac{\psi_1'}{\phi'} \\ &- \left[E_3 I_3 + \frac{X_3 t_3 Z_3}{2} + X_4 t_3 Z_4\right] \frac{\psi_2'}{\phi'}\end{aligned} \tag{52}$$

To compute the loss factor for the four-layer system it is necessary to consider material properties to consist of real and imaginary parts. Thus,

$$E_3 = E_3(1 + i\eta_3) \tag{53}$$

and

$$G_3 = G_3(1 + i\eta_3) \tag{54}$$

where

$$i = \sqrt{-1}$$

Using Equations (53) and (54) in Equation (52) results in

$$\overline{EI} = EI_{real} + EI_{imag}, \tag{55}$$

The intermediate manipulations required to determine EI_{real} and EI_{imag} are straightforward but very lengthy; consequently, they are not included. The system modal loss factor, η_m, is found from

$$\eta_m = \frac{EI_{imag}}{EI_{real}} \tag{56}$$

The modal frequency for Nth mode of vibration, is calculated by:

$$f_N = \frac{1}{2\pi} \times K_N^2 \sqrt{\frac{\overline{EI_{real}}\, g}{\sum_{k=1}^{4} H_k \rho_k}} \tag{57}$$

where:
K^2 = wave number; = $K_N^2 = \frac{(N\pi)^2}{L^2}$
H_k = k^{th} layer thickness;
ρ_k = k^{th} layer density, mass/limit volume;
N = mode number; and
g = acceleration of gravity.

In practice the complex modulus is evaluated for the given temperature and an estimated modal frequency, f_e. The modal frequency is calculated from f_N and compared to the convergence criteria.

$$\left|1 - \frac{f_e}{f_N}\right| \leq \epsilon_{FREQ} = 0.01 \tag{58}$$

If this condition is not met, the new estimated frequency is taken as the old calculated frequency and the process repeated.

3.0 Comparison of Response

The peak amplitude response for a one degree of freedom system undergoing sinusoidal excitation of amplitude f_0 is

$$X_{peak} = \frac{f_0}{k\eta} = \frac{f_0}{m(2\pi f)^2\eta} \tag{59}$$

and the ratio

$$\frac{X_{peakundamp}}{X_{peakdamp}} = \frac{m_d}{m_u} \times \left(\frac{f_d}{f_u}\right)^2 \times \frac{\eta_d}{\eta_u} \tag{60}$$

The root-mean-square amplitude response W_{rms}, (equivalently, of a SS beam where the force is spatially sinusoidal and temporally random) is obtained by using the equation derived in [6]; that is

$$W_{rms} = \frac{\pi \overline{F}(w)}{2\sqrt{2}m^{1/4}K^{3/4}\eta^{1/2}} \times \left[\frac{1+\sqrt{1+\eta^2}}{\sqrt{1+\eta^2}}\right] \tag{61}$$

Noting that

$$m(w)^2 = k = m(2\pi f)^2 \tag{62}$$

Then the ratio between the responses of the damped and undamped (with and without the damping treatment) is found from

$$RMS = \frac{(W_{rms}/\overline{F}(w))_u}{(W_{rms}/\overline{F}(w))_d} = \frac{m_d}{m_u} \times \frac{\sqrt{1+\eta_d^2}}{\sqrt{1+\eta_u^2}} \times \frac{\left[1+\sqrt{1+\eta_u^2}\right]}{\left[1+\sqrt{1+\eta_d^2}\right]} \times \sqrt{\frac{\eta_d}{\eta_u}} \times \left(\frac{f_d}{f_u}\right)^{\frac{3}{2}} \tag{63}$$

where the subscript "u" refers to the base structure by itself and "d" represents the response with the damping treatment.

4.0 CALCULATIONS

Figure 4 presents the flow of the computations. The characteristics of the undamped baseline beam and the characteristics of the candidate damping treatment, including parameters used to described the viscoelastic damping material, are input. The frequency of the baseline beam is calculated. For a specified temperature, the value of temperature shift function is calculated. The reduced frequency is calculated using an estimated frequency; then, the shear modulus of the viscoelastic layer is calculated. The equations derived above are used to calculate modal damping and frequency; if the calculated frequency is identical to the one used to calculate the VEM shear modulus, the results are consistent. If the convergence criteria is not met, the calculation is

iterated for a an improved value of estimated frequency. Once convergence is achieved for a temperature, the RMS and PEAK values are calculated.

To obtain a better understanding of the important parameters for an SOD system, sensitivity studies were run in which the base beam was held constant while the thickness of the Stand-Off layer, viscoelastic layer, and constraining layer were varied by 20 percent. In addition, the modulus of the constraining layer was also varied by 20 percent. Each variation was made independent of the other three. The initial model used for this study is shown in Figure 5 and consists of a .080 inch thick stand-off layer, a .005 inch layer of 3M Co. Y- 966 viscoelastic, and a .010 inch thick aluminum constraining layer. The results of the sensitivity study are presented in Table 1 and indicate that the most important parameter for increased performance is the spacer thickness. To a lesser extent, the thickness and modulus of the constraining layer also provide an increase in performance. The least sensitive parameter in this study is the thickness of the damping layer. In addition, the temperature for optimum performance is only slightly influenced by these parameters.

A second analytical study was conducted to determine the performance sensitivity of the SOD system to variations of the shear modulus of the Stand- Off layer. This was carried out using the configuration shown in Figure 5 and the results are presented in Table 2 and Figure 6. This study indicates that the SOD system investigated is relatively insensitive to large changes in the shear modulus of the Stand-Off layers. In addition, the temperature for optimum performance is shifted up as the shear modulus of the stand-off layer is decreased (Table 2).

5.0 HARDWARE DEMONSTRATION

To verify the Stand-Off damping treatment analysis and concept, a practical demonstration was undertaken. The single span generic aircraft skin-stringer- frame panel, illustrated in Figure 7, was selected as the test article.

A dynamic survey was performed on the undamped test article to characterize the important modal parameters required to design a damping system. This was done by applying a known excitation load to the panel and measuring its response. For this case, an impact load was used to excite the panel at specific locations and its response was measured using a accelerometer located at a second point. These signals were input to a two channel digital signal analyzer in order to generate the inertance frequency response function between the test points. Figure 8 illustrates a typical driving point frequency response function for the undamped test article. It can be seen from the FRF that a number of resonant modes with low damping values are present in the 200 Hz to 800 Hz frequency range.

In order to effectively design a damping treatment for the test article, it was necessary to determine the deformation patterns for those modes of interest. This was accomplished by comparing the FRF between 336 different points on the panel. The relative magnitude and phase angle between all points for each resonant mode was then used to determine the deformation patterns for specific resonant models, as illustrated in Figure 9.

Based on the modal study, the fundamental panel bending model (236 Hz) was selected as the target model for correlation. An equivalent beam model compatible with the input requirements of the program was developed. The model maintained the thickness and mass distribution of the skin component but altered the Young's modulus to account for Poisson's stiffening. An equivalent simply supported beam length of five (5) inches was determined using fourth order beam and plate theory.

Two damping configurations, shown in Figure 10, were analyzed, fabricated, applied to the test panel, and tested. The first treatment was a conventional constrained layer viscoelastic material system consisting of a .005 inch damping layer and a 0.010 inch aluminum constraining layer applied to the base. The second treatment was a partial coverage SOD system with a .080 inch spacer introduced between the base structure and the viscoelastic damping layer. The predicted performance for these treatments is shown in Figures 11 and 12.

Figures 13 and 14 compare the measured driving point FRF for the test article with and without the indicated configuration at 74 degrees F. These graphs illustrate the overall vibratory reduction obtained for each of the damping designs. The same measurements were made at different temperatures and the loss factor for the target mode was determined using the half power band width technique. The measured modal loss factors at each test temperature are included in Figures 11 and 12 for the respective treatments.

These test results show excellent correlation between the predicted and measured modal loss factor over the test temperature range. Further, the experimental results confirm that modal loss factors in excess of 0.10 are achieved from approximately 60 degrees F. up to the maximum test temperature.

6.0 CONCLUSIONS

The analytical and experimental results presented clearly demonstrate the impressive vibratory suppression benefits a properly configured Stand-Off-Damping system can provide when compared to a conventional distributed damping systems. This performance is achieved with an add-on system that imposes only modest space and weight requirements to the overall system.

The analytical model provides a good first approximation for predicting the modal loss factor for the fundamental mode over a wide temperature range. Additional development to expand the analytical model to accommodate different boundary conditions and multiple damping/constraining layers would greatly increase its utility.

7.0 REFERENCES

1. Ross, D., Ungar, E. E., and Kerwin, E. M., "Structural Damping", J. E. Ruzicka, Ed., American Society of Mechanical Engineers, 1959.
2. Snowdon, J. C., "Vibration and Shock in Damped Mechanical Systems", John Wiley & Sons, 1968.
3. Fung, Y. C., "A First Course In Continuum Mechanics", Second Edition, Prentice-

Hall, Inc., Englewood Cliffs, New Jersey, 1977.
4. Byars, E. F., and Snyder, R. D., "Engineering Mechanics of Deformable Bodies", Second Edition, International Textbook Company, Scranton, Pennsylvania, 1969.
5. Ungar, E. E., and Kerwin, Jr., E. M., "Loss Factors of Viscoelastic Systems in Terms of Energy Concepts," The Journal of the Acoustical Society of America, Vol. 34, No. 7, pp. 954-957, July 1962.
6. Nashif, A., and Jones, D., Henderson, J. P., "Vibration Damping", John Wiley & Sons, 1985.
7. Rogers, L., Notes from Vibration Damping Short Course, University of Dayton Research Institute, Sections 6 and 7, November 1987.
8. Miles, R. N., "The Prediction of the Damping Effectiveness of Multiple Constrained Layer Damping Treatments", Presented at Acoustical Society of America, Massachusetts Institute of Technology, June 11-15, 1979.

SENSITIVITY

H_2 (in.)	H_3 (in.)	H_4 (in.)	E_4 (psi)	X_{RMSU}/X_{RMSD} (MAX)	TEMP (°F)	% CHANGE
0.080	0.005	0.010	10E6	21.68	100	BASE
0.096	0.005	0.010	10E6	25.92	100	19.56
0.080	0.006	0.010	10E6	21.96	95	1.29
0.080	0.005	0.012	10E6	24.61	95	13.51
0.080	0.005	0.010	12E6	24.16	95	11.44

TABLE 1

SENSITIVITY

G_2 (psi)	X_{RMSU}/X_{RMSD} (MAX)	TEMP (°F)
200,000	21.68	100
160,000	21.64	100
83,000	21.45	100
64,000	21.34	100
32,000	20.85	100
16,000	19.95	100
8,000	18.41	100
4,000	16.08	105
2,000	13.06	110
1,000	9.88	120

TABLE 2

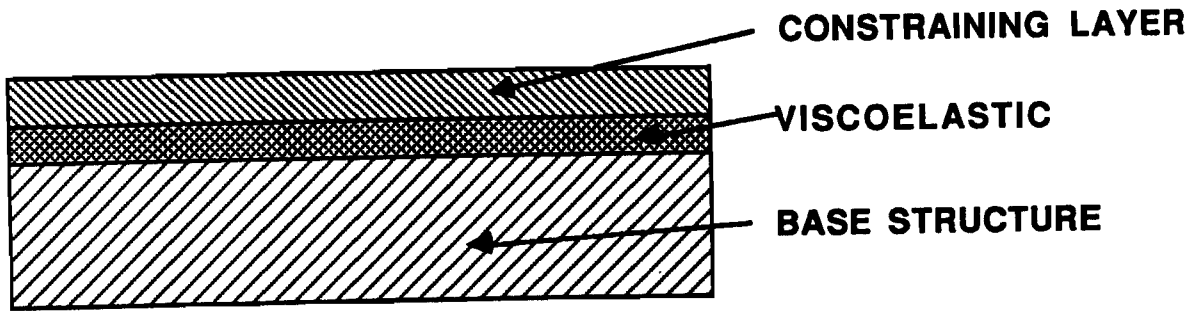

1a

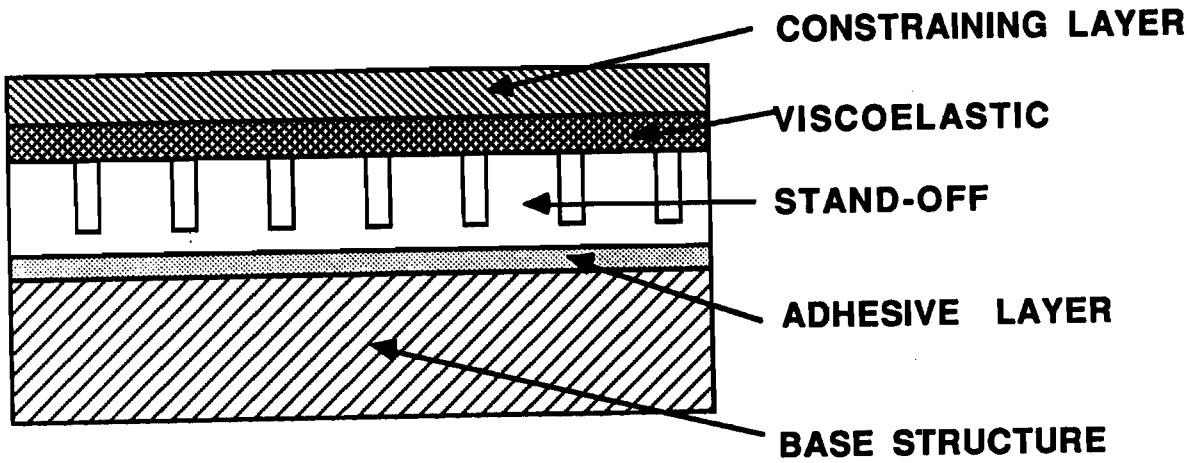

1b

Figure 1 - Conventional and Stand-Off Constrained Layer Damping Systems

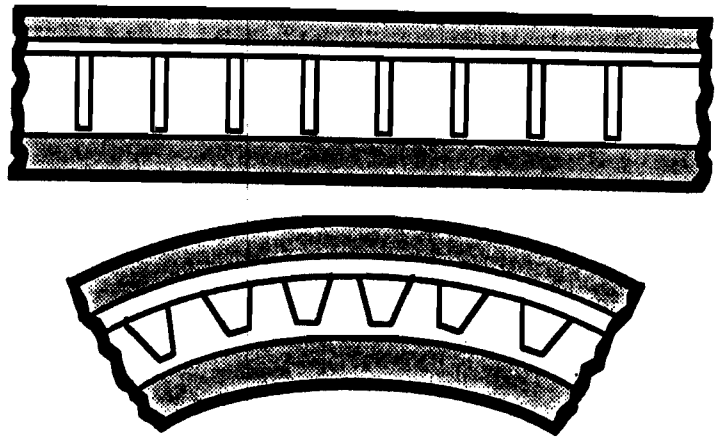

Figure 2 - Deformed Stand-Off System

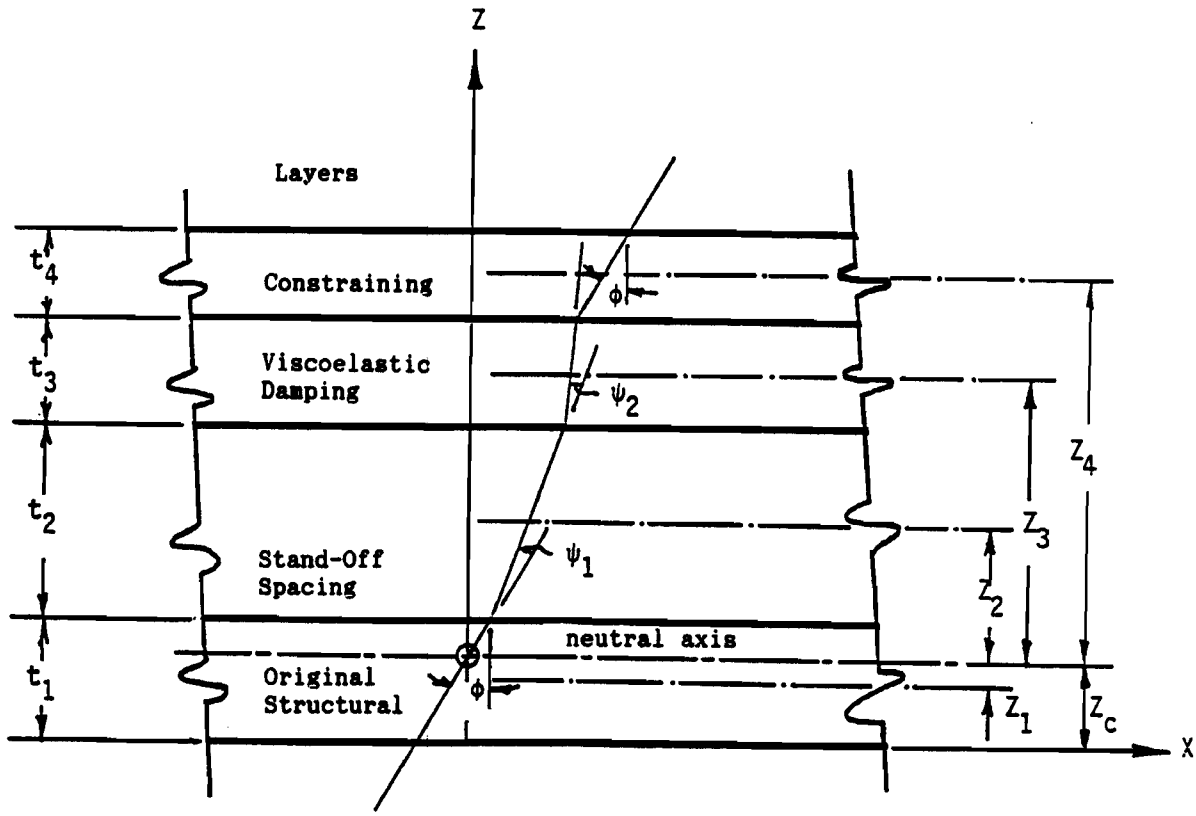

Figure 3 - Schematic of Four-Layer Viscoelastic Constrained Layer Damping System

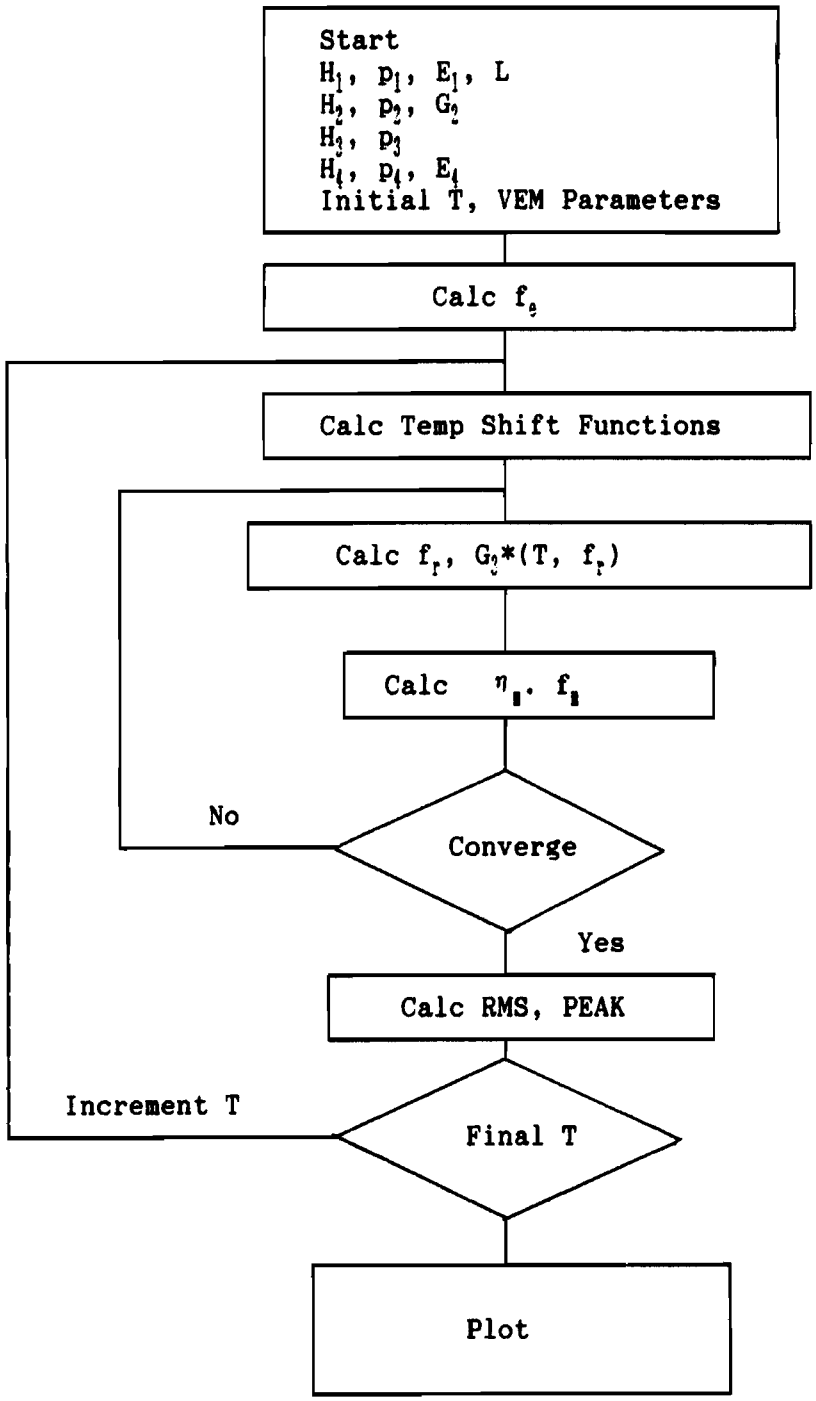

Figure 4

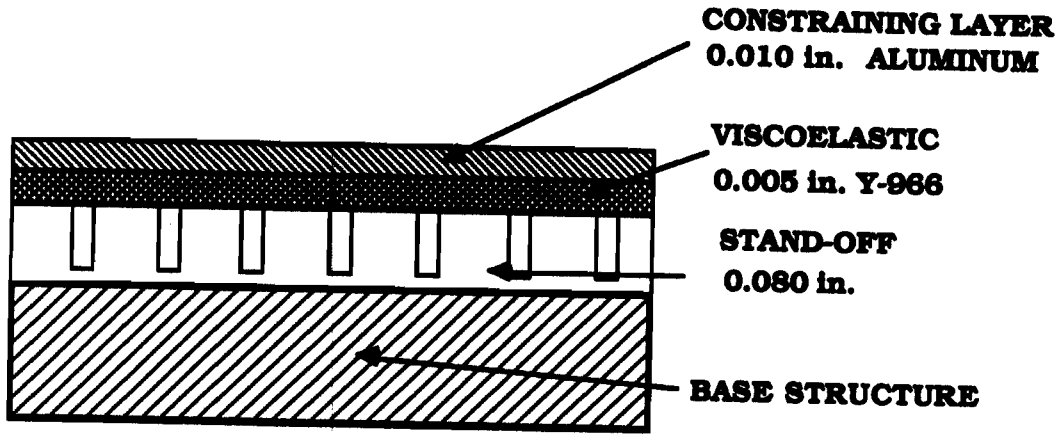

Figure 5

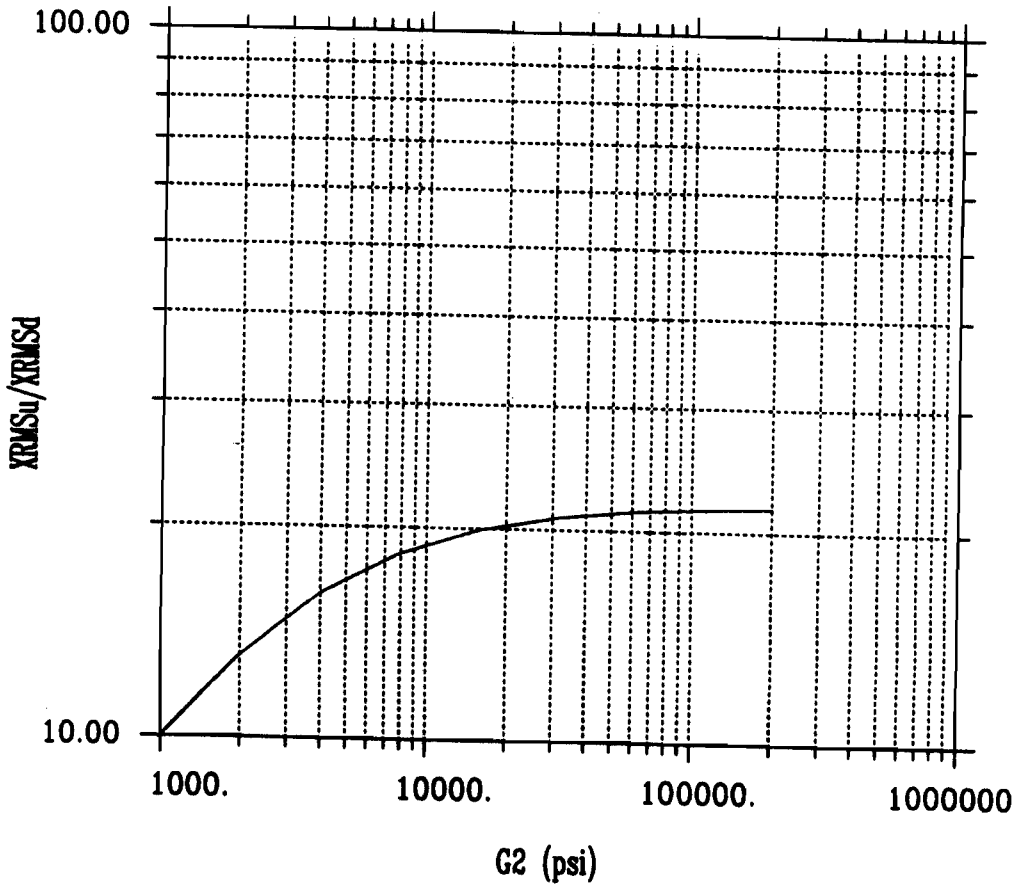

Figure 6 - Influence of Stand-Off Modulus on RMS Response Ratio

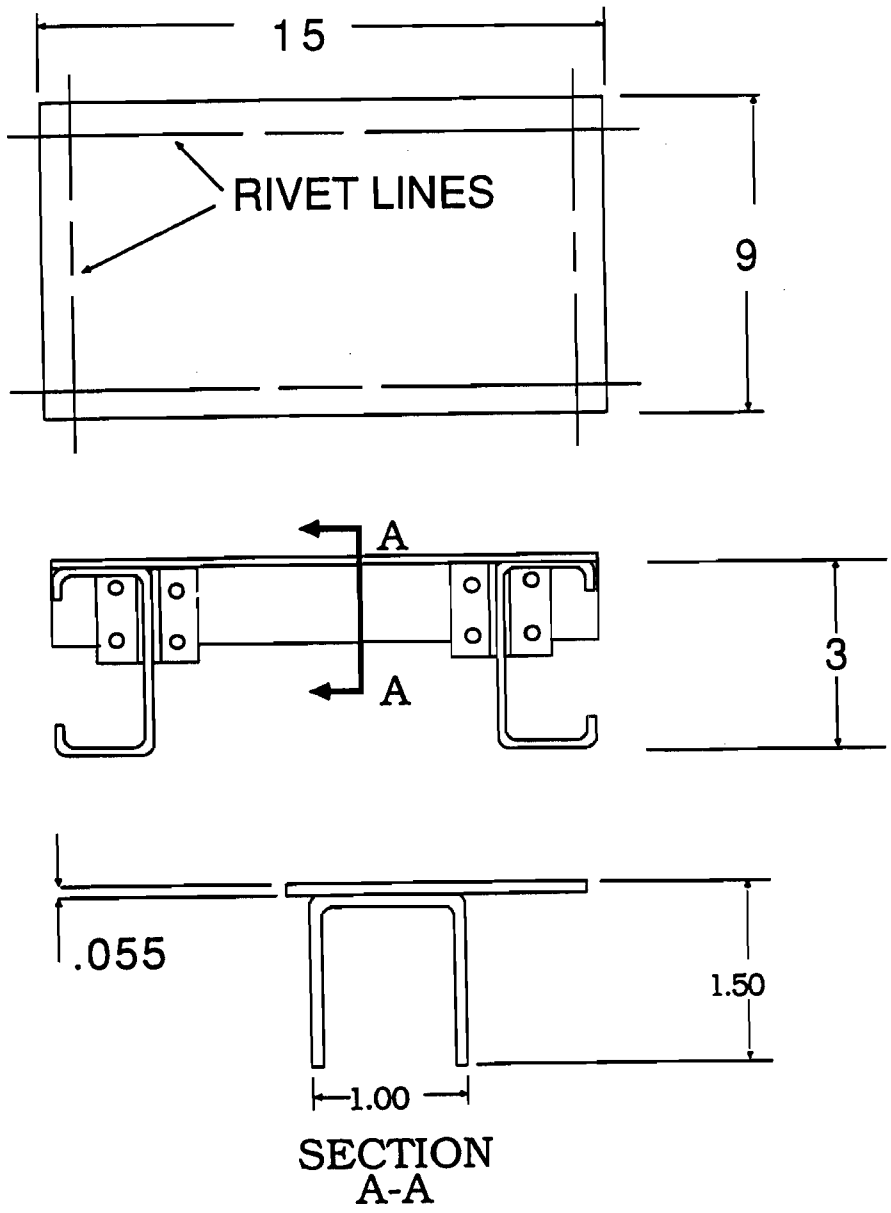

Figure 7

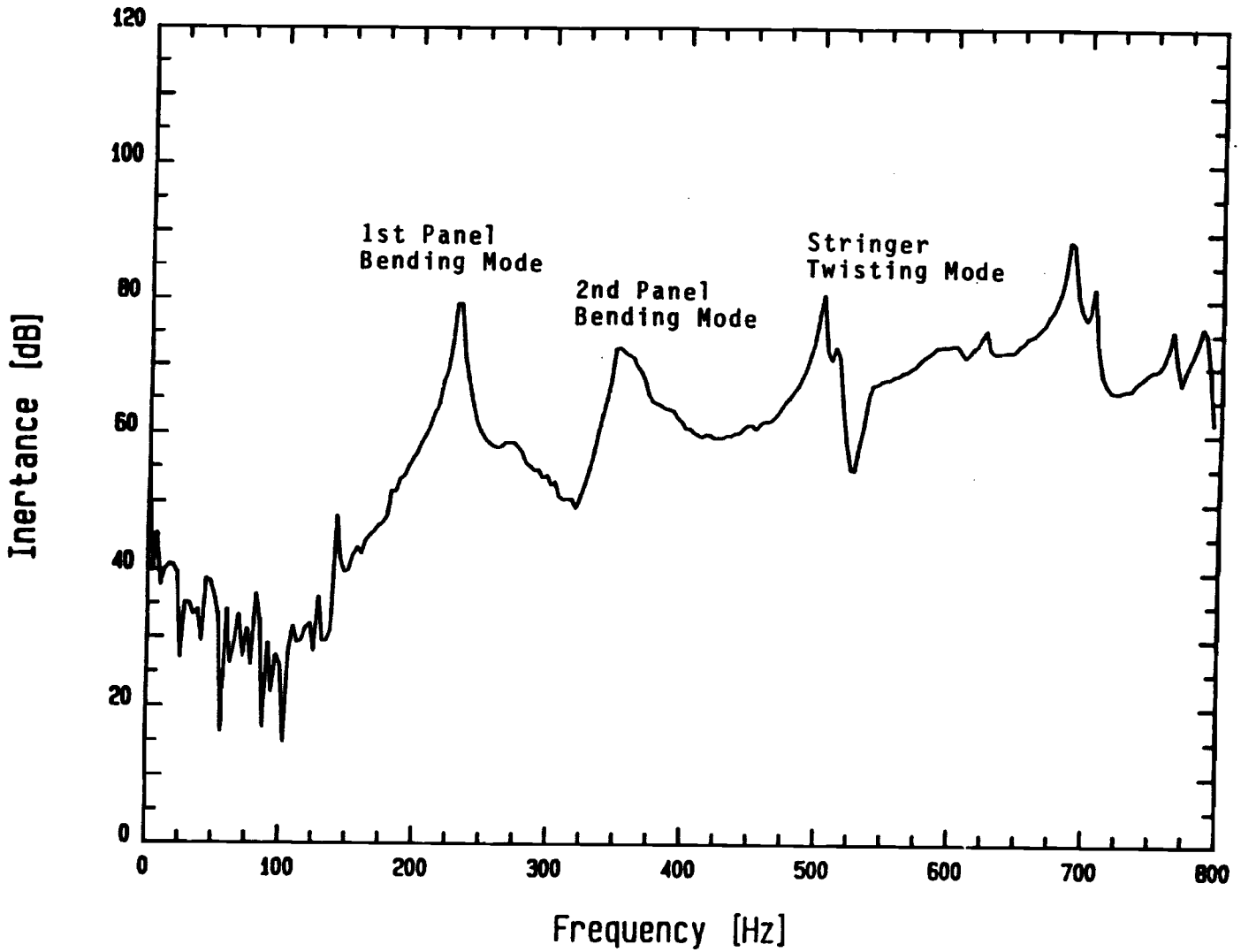

Figure 8 - Frequency Response for Bare Test Panel

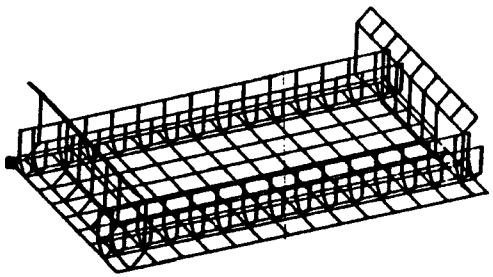

Undeformed Test Article

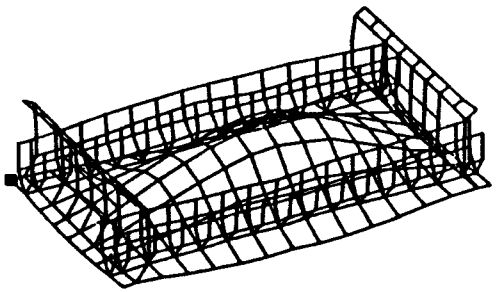

1st Bending Mode 236 Hz

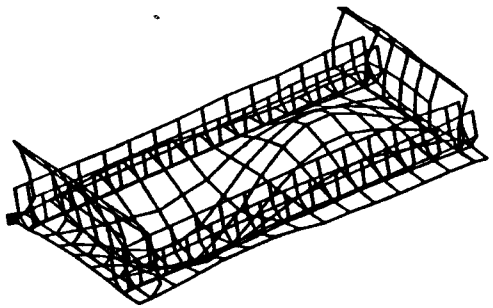

2nd Bending Mode 331 Hz

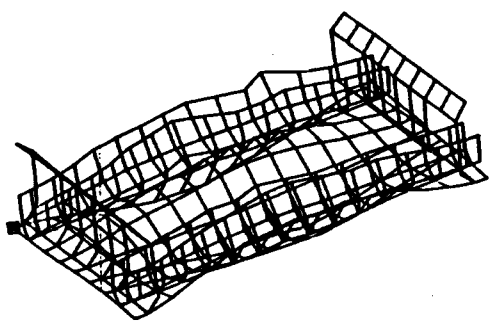

Stringer Twisting Mode 510 Hz

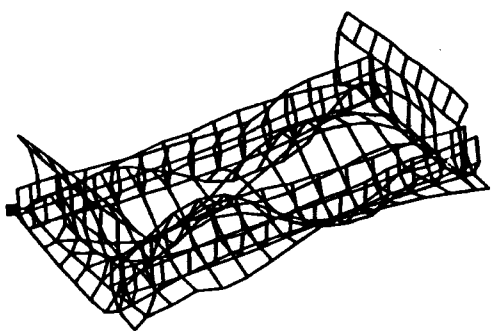

Stringer Twisting Mode 726 Hz

Figure 9

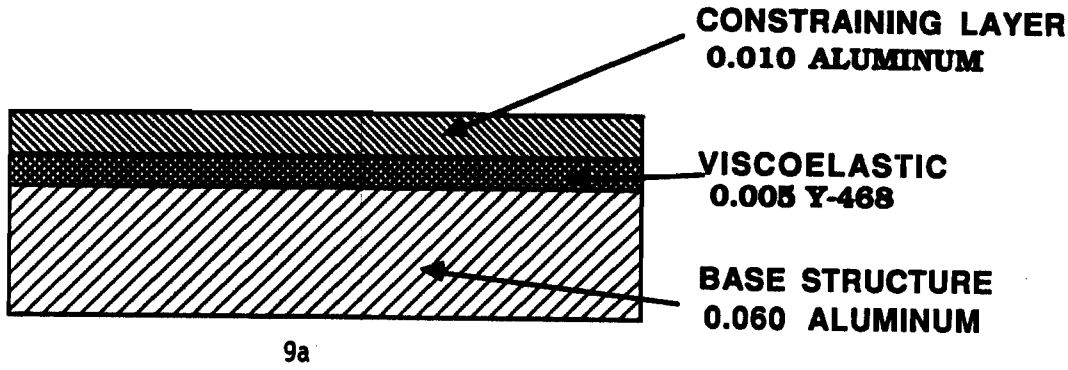

9a

Conventional Constrained Layer System

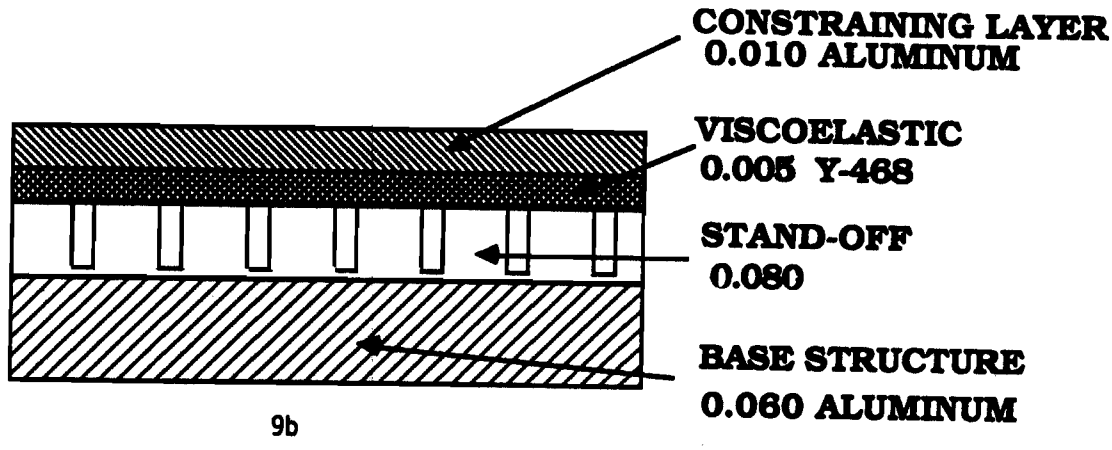

9b

Stand-Off Constrained Layer System

Figure 10

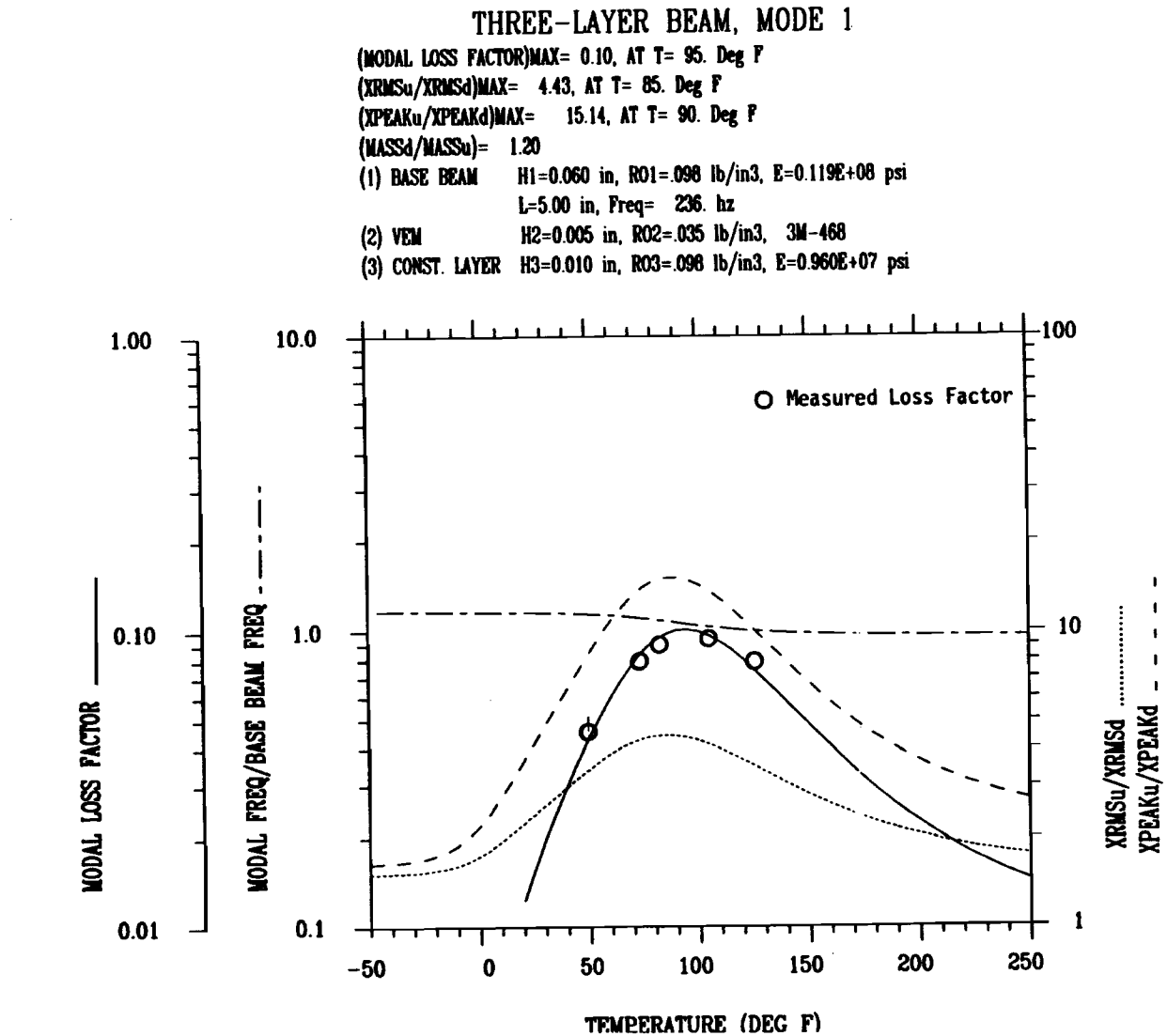

Figure 11- Comparison of Predicted and Measured Loss Factor for 1st Bending Mode with Conventional Constrained Layer

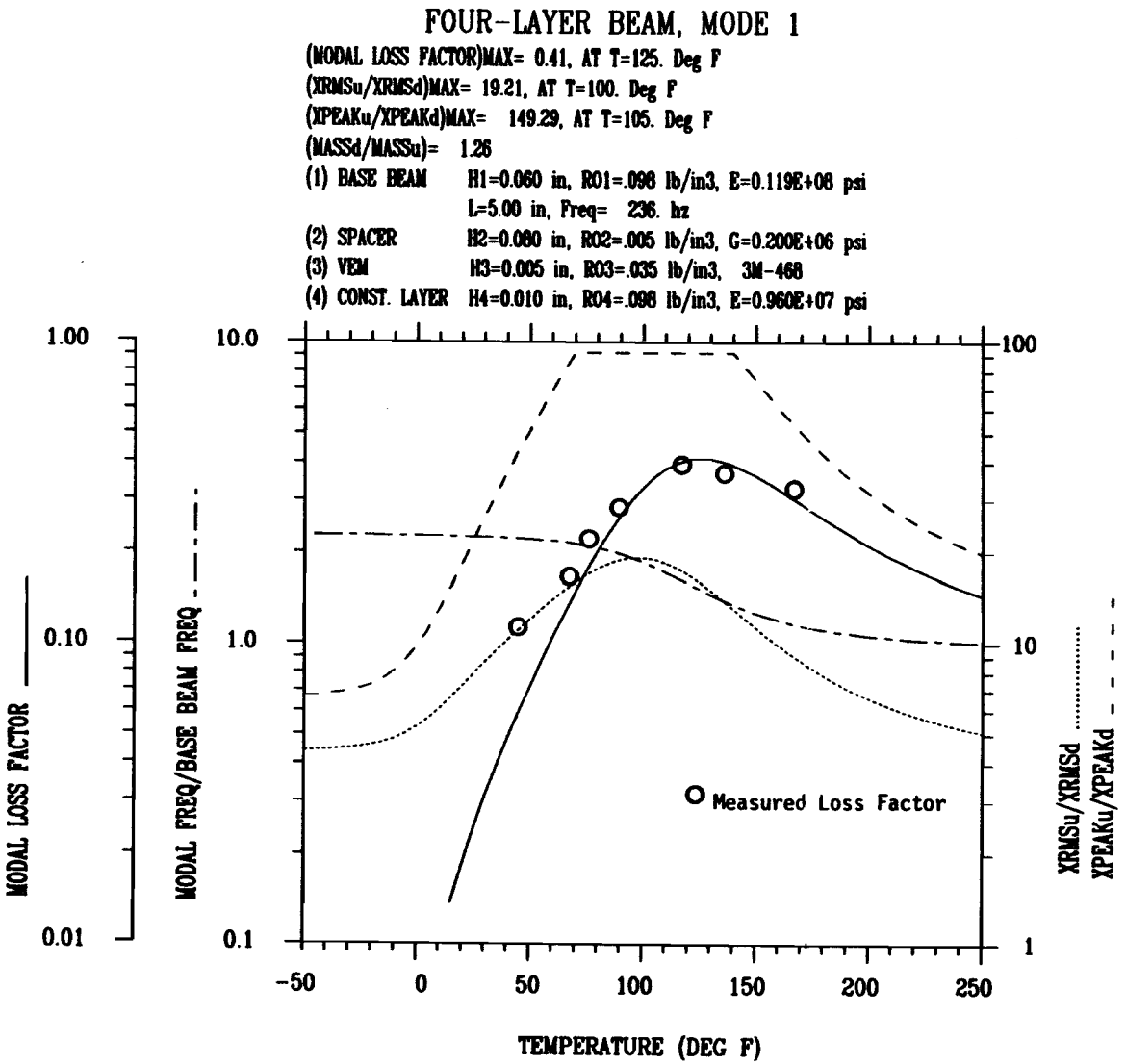

Figure 12 - Comparison of Predicted and Measured Loss Factor for 1st Bending Mode of Test Panel with SOD System

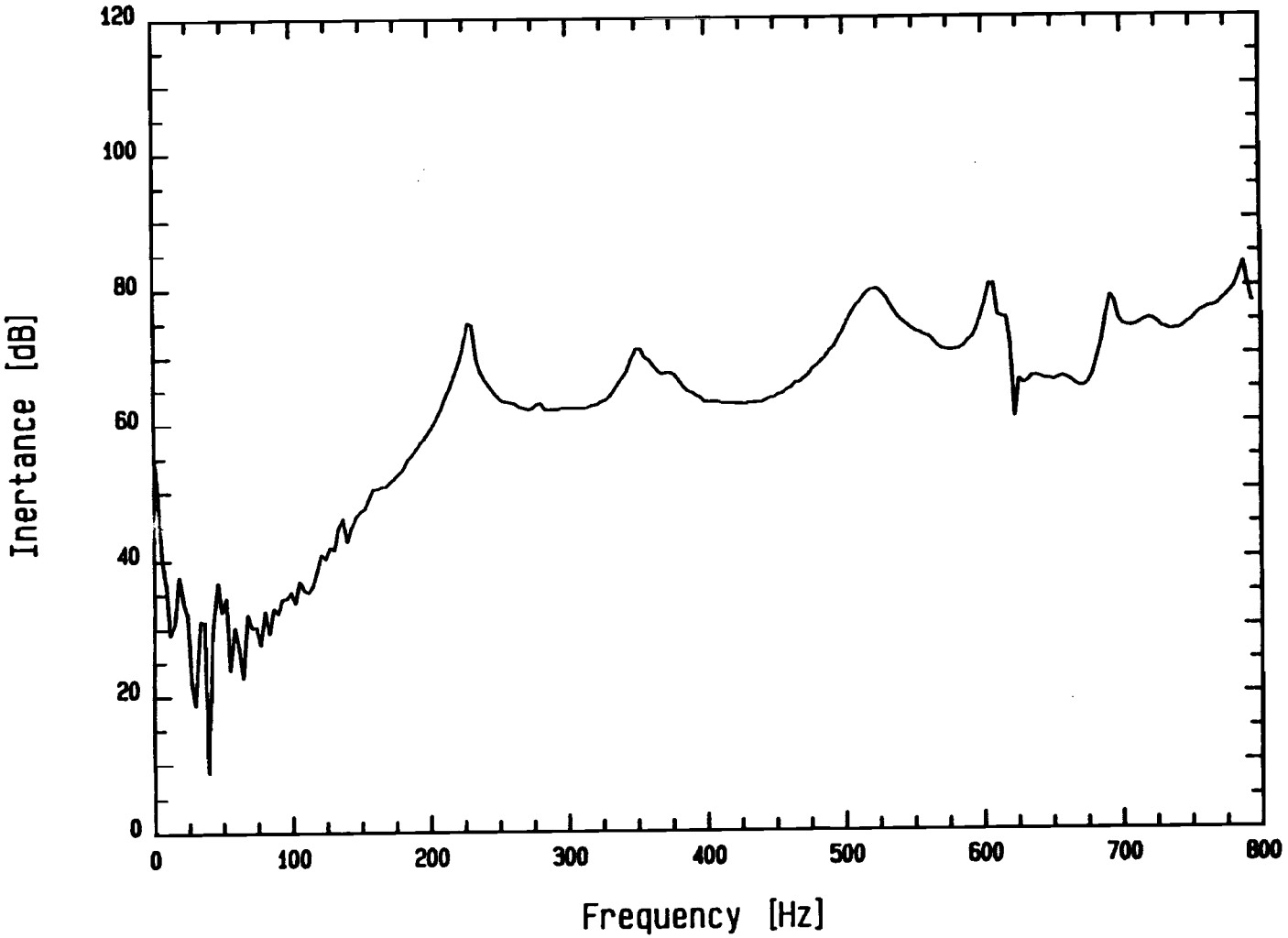

Figure 13 - Driving Point Frequency Response for Test Article With Conventional Constrained Layer Treatment at 74 Degrees F.

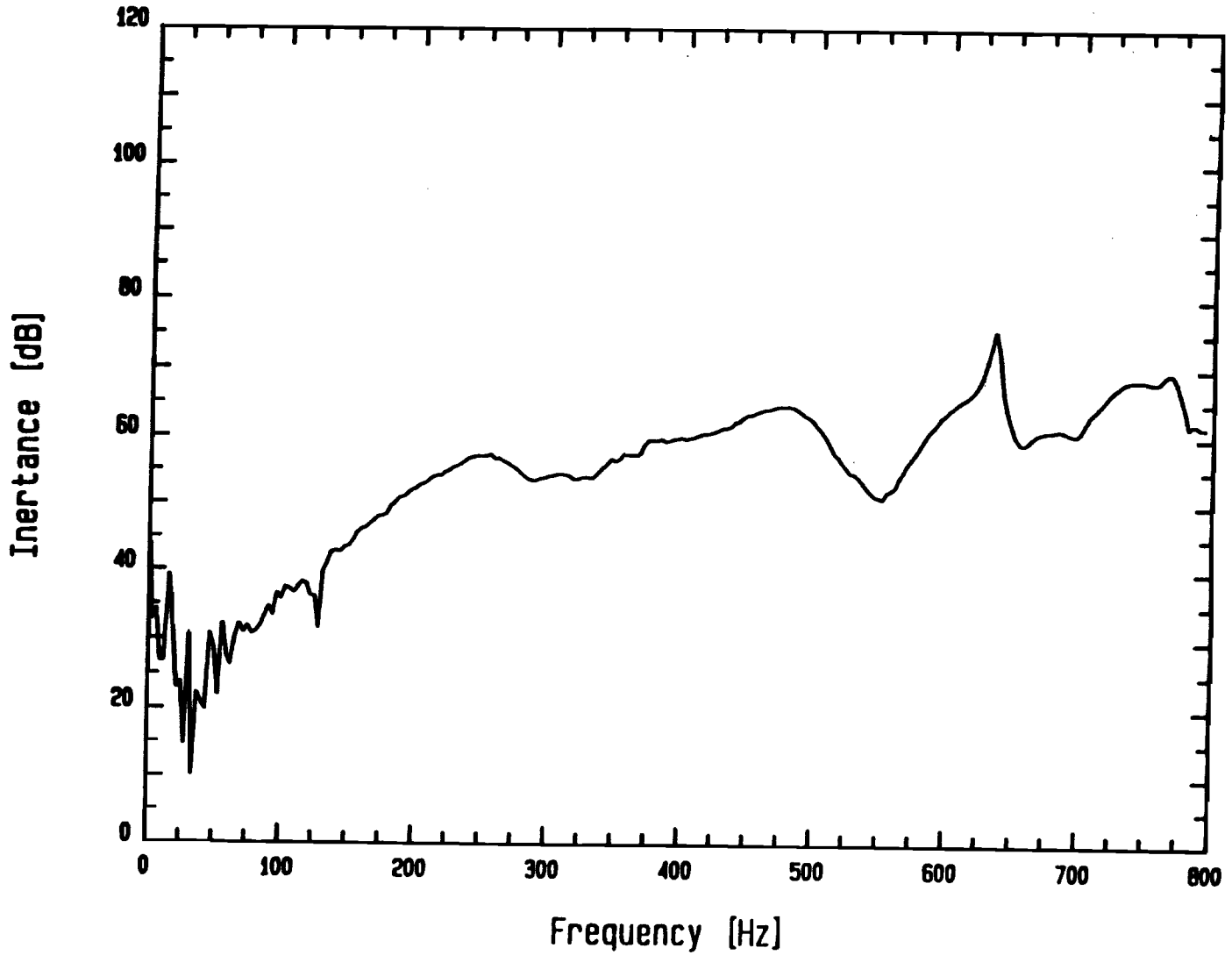

Figure 14 - Frequency Response For Test Panel With Stand-Off Damping System at 74 Degrees F.